# Fabrication of Novel Nitrogen-Doped Graphene−Hollow AuPd Nanoparticle Hybrid Films for the Highly Efficient Electrocatalytic Reduction of H$_2$O$_2$

Lei Shang, Baizhao Zeng, and Faqiong Zhao*

Key Laboratory of Analytical Chemistry for Biology and Medicine (Ministry of Education), College of Chemistry and Molecular Sciences, Wuhan University, Wuhan 430072, Hubei Province, P. R. China

Ⓢ *Supporting Information*
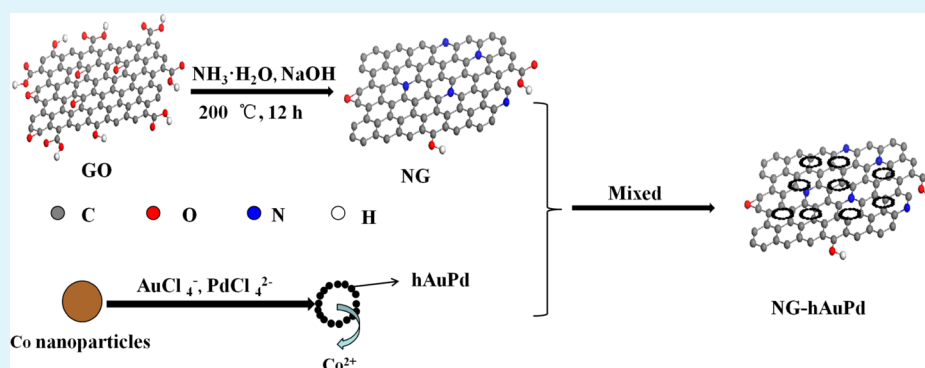
ABSTRACT: Hollow AuPd (hAuPd) alloy nanoparticles (NPs) were prepared through simultaneous reduction of HAuCl$_4$ and Na$_2$PdCl$_4$ using Co NPs as sacrificial template (i.e., reductant). Then, the hAuPd NPs were assembled on nitrogen-doped graphene (NG) to prepare an NG−hAuPd hybrid film. The obtained NG−hAuPd composite showed higher electrocatalytic activity toward the reduction of H$_2$O$_2$, compared with graphene−hAuPd hybrid, NG−solid AuPd hybrid, and hAuPd NPs. The enhanced performance was related to the hollow structure of hAuPd NPs and the synergistic effect between NG and hAuPd NPs. Under optimum conditions, the NG−hAuPd hybrid film showed a linear response to H$_2$O$_2$ in the range of 0.1−20 μM, with a sensitivity of 5095.5 μA mM^{-1} cm^{-2} and a comparable detection limit of 0.02 μM (S/N = 3). These results demonstrated that the NG−hAuPd composite was a promising electrocatalytic material for constructing sensors, etc.

KEYWORDS: *nitrogen-doped graphene, hollow AuPd nanoparticles, H$_2$O$_2$, electrocatalysis, alloy*

INTRODUCTION

Hydrogen peroxide plays an important role in clinical, food, pharmaceutical, and environmental fields,[1,2] so the precise and rapid detection of H$_2$O$_2$ is essential. Recently, the Pd nanoparticles (NPs) based nonenzymatic H$_2$O$_2$ sensors have drawn wide attention, because Pd showed excellent catalytic activity toward H$_2$O$_2$ and did not have the drawbacks of high cost and poor stability of enzymes.[3−6] For example, Jia et al.[4] reported a novel sensing platform for H$_2$O$_2$ based on immobilized palladium−helical carbon nanofiber (Pd−HCNF) hybrid nanostructures with Nafion on a glassy carbon electrode (GCE). The modified electrode exhibited sensitive response toward H$_2$O$_2$. Bian et al.[6] loaded Pd NPs on novel mesoporous carbon nanospheres (MCNs), which possessed high specific surface area and large pore volume. The resulting Pd NPs/MCNs hybrid exhibited good electrocatalytic activity toward the reduction of H$_2$O$_2$, excellent stability and anti-interference capability for the detection of H$_2$O$_2$. Furthermore, the addition of Au to Pd reportedly promoted overall catalytic activity, selectivity, and stability of Pd.[7−10] For instance, Yang et al.[11] synthesized Au−Pd alloy NPs supported on carbon fiber

cloth (Au−Pd NPs/CFC), and the obtained hybrid exhibited excellent catalytic property and good stability for H$_2$O$_2$ electroreduction in acid solution, and it outperformed pure Au and Pd catalyst supported on CFC.

On the other hand, the catalytic performance is largely dependent on catalyst structures. Currently, synthesis and application of metal NPs with interior cavities and controlled shell architectures are attracting considerable interest. In comparison with their solid counterparts, hollow NPs have larger surface area and lower density, and thus are highly desirable nanostructures for catalysis and sensing.[12−15] Wang et al.[12] reported the facile synthesis of PtPd bimetallic nanocages with a hollow interior by selective chemical etching of Pd cores of dendritic Pt-on-Pd NPs. The obtained PtPd nanocages showed superior catalytic activity for methanol oxidation reaction compared with the original Pt-on-Pd nanodendrites. Hong et al.[13] synthesized PdPt alloy nanocrystals (NCs) with
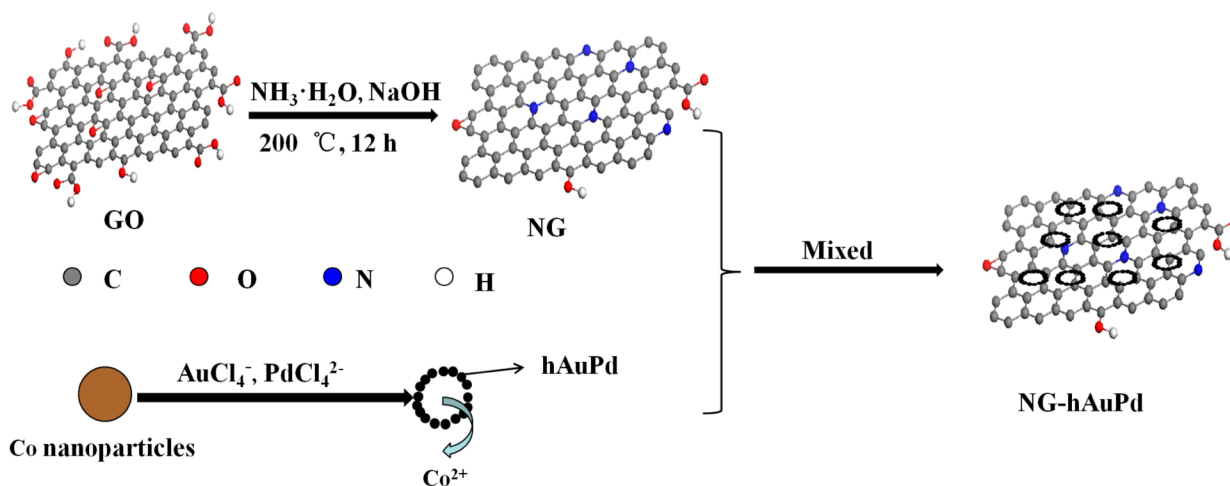
Figure 1. Scheme of the preparation of NG−hAuPd hybrid film.

hollow structures by a galvanic replacement method using uniform Pd NPs as sacrificial template, and the obtained hollow NCs exhibited considerably enhanced catalytic activity to oxygen reduction. However, so far, hollow AuPd (hAuPd) NPs have never been used for the electrocatalytic reduction of H_2O_2.

As is well-known, to enhance the catalytic efficiency of an electrocatalyst, a suitable support is required, which can promote the efficient dispersion of catalyst particles. Owing to its unique physical and chemical properties, graphene has opened a new avenue for utilizing carbon supports.[16−20] When PtNi alloy NPs were loaded on graphene nanosheets, they showed significantly improved performance in nonenzymatic amperometric detection of glucose.[17] Chen et al.[19] synthesized ultrafine AuPd NPs monodispersed on graphene by a one-pot green method, and the as-prepared AuPd NPs/graphene hybrid exhibited a high activity toward the reduction of 4-nitrophenol. Furthermore, several reports have shown that the electrochemical behavior and electron transport capability of graphene can be improved further by doping N atoms.[21−25] Thus, nitrogen-doped graphene (NG) would be a better support than graphene for loading catalyst particles. For example, the catalytic activity of Pt NPs loaded on NG was much higher than that loaded on undoped graphene for oxygen reaction[26] and methanol oxidation.[27] However, hitherto, there are no reports on the controllable assembly of hAuPd NPs on NG films.

Herein, we prepared an NG−hAuPd hybrid material by assembling hAuPd NPs on NG. The resulting nanohybrid showed remarkable electrocatalytic activity toward the reduction of H_2O_2.

■ EXPERIMENTAL SECTION

Reagents. $HAuCl_4·4H_2O$, Na_2PdCl_4, $CoCl_2·6H_2O$, $NH_3·H_2O$, NaOH, sodium citrate dehydrate, $NaBH_4$, $Na_2HPO_4·12H_2O$, $NaH_2PO_4·2H_2O$, uric acid, ascorbic acid, and glucose were purchased from Sinopharm Chemical Reagent Co. Ltd. (Shanghai, China). Graphene oxide (GO) came from Xianfeng Reagent Co. Ltd. (Nanjing, China). Other reagents were of analytical grade and used as received. The water used was redistilled.

Apparatus. Cyclic voltammetry and electrochemical impedance spectroscopy (EIS) were performed with a CHI 604D electrochemical workstation (CH Instrument Company, Shanghai, China). The amperometric measurement was carried out with a CHI832C electrochemical workstation. A conventional three-electrode system was adopted. The working electrode was a modified GCE (diameter: 2

mm), and the auxiliary and reference electrodes were a platinum wire and a saturated calomel electrode (SCE), respectively. The transmission electron microscope (TEM) images were obtained using a JEM-2100 (HR) TEM (JEOL Ltd., Japan). The energy dispersive X-ray spectroscopy (EDX) was obtained using a Hitachi X-650 SEM (Hitachi Co., Japan). X-ray diffraction data (XRD) were recorded with a Bruker D8 diffractometer (Germany) using Cu $K\alpha$ radiation (40 kV, 40 mA) with a Ni filter. X-ray photoelectron spectroscopy (XPS) analysis was carried out on a KRATOS XSAM800 X-ray photoelectron spectrometer with Mg $K\alpha$ X-ray radiation for excitation.

Preparation of NG−hAuPd Hybrid Film. The preparation of NG−hAuPd hybrid film is illustrated in Figure 1. First, NG was prepared through a solvothermal process.[23] In a typical synthesis, 40 mg of GO was dispersed in 25 mL of water, and then 15 mL of $NH_3·H_2O$ (25%) and 300 mg of NaOH were added to create a homogeneous solution. This mixture was transferred to a 50 mL Teflon-lined autoclave for reaction at 200 °C for 12 h. Afterward, NG was collected by centrifugation and washed with HCl solution to remove residual NH_3, followed by water and ethanol repeatedly for six times. The final product was dried in a vacuum oven at 70 °C for 3 h. Undoped graphene (G) was prepared by the same method, but $NH_3·H_2O$ was absent. Second, hollow Au1Pd4 (hAu1Pd4) NPs were fabricated as follows: 4.25 mg of $CoCl_2·6H_2O$ and 10.0 mg of trisodium citrate dehydrate were dispersed in 25 mL of water, and the mixture was stirred under a nitrogen atmosphere at room temperature for 30 min. Then, 10 mL (1 mg mL^{-1}, in water) of $NaBH_4$ was added and the solution changed from colorless to dark brown, demonstrating the formation of Co NPs. This solution was further stirred under nitrogen for about 30 min until hydrogen evolution ceased to ensure all $NaBH_4$ had hydrolyzed. Then, 80 μL of 25 mM $HAuCl_4·4H_2O$ and 320 μL of 25 mM Na_2PdCl_4 were synchronously dropwise added to the above solution. Upon completion, the solution was stirred for another 15 min, allowing the full reaction between Co NPs and $HAuCl_4$ and Na_2PdCl_4. Then, the nitrogen flow was stopped and the vessel was opened to the ambient conditions to oxidize any remaining Co metal in the solution. Subsequently, the solution was centrifuged to eliminate the dissolved Co template, which was oxidized by $HAuCl_4$ and Na_2PdCl_4 to Co(II). The sediment was dispersed in 5 mL of water. Similarly, other hAuPd materials were synthesized by varying the molar ratio of $HAuCl_4$ and Na_2PdCl_4 (such as 1:0, 1:2, 1:6, and 0:1). It should be pointed out that the total concentration of $HAuCl_4·4H_2O$ and Na_2PdCl_4 in the mixed solution was kept at 0.4 mM. The obtained hollow NPs were donated as hAu1Pd4, hAu, hAu1Pd2, hAu1Pd6, and hPd NPs, respectively. Solid Au1Pd4 (sAuPd) NPs were synthesized through a similar method, but 10 mL of $NaBH_4$ was replaced by 1 mL of 0.1 M ascorbic acid and the Co template was absent. Third, for the preparation of NG (or G)−AuPd hybrid films, the obtained AuPd NPs suspension was mixed with 3 mg of NG or G.
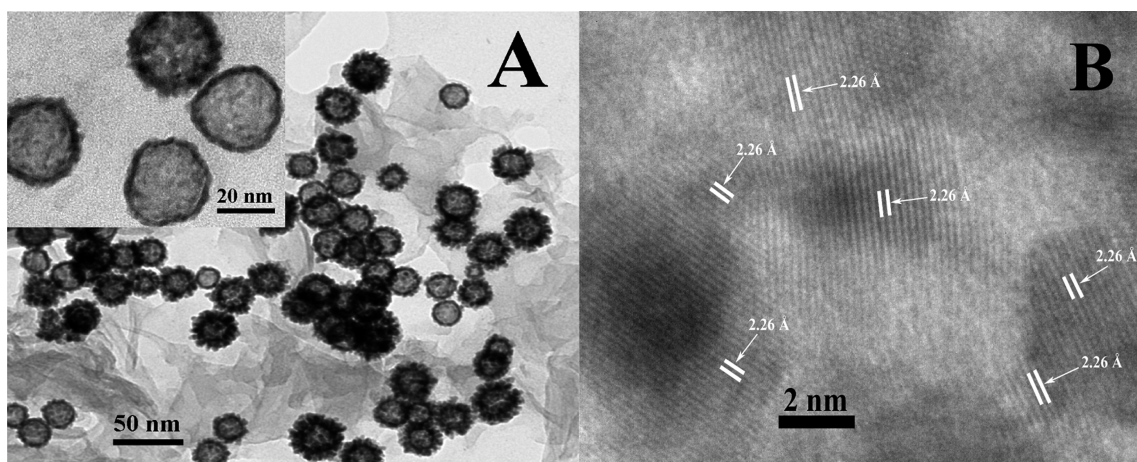
Figure 2. TEM image (A) and HRTEM image (B) of hAuPd NPs assembled on NG. Inset: the magnified TEM image of hAuPd NPs assembled on NG.
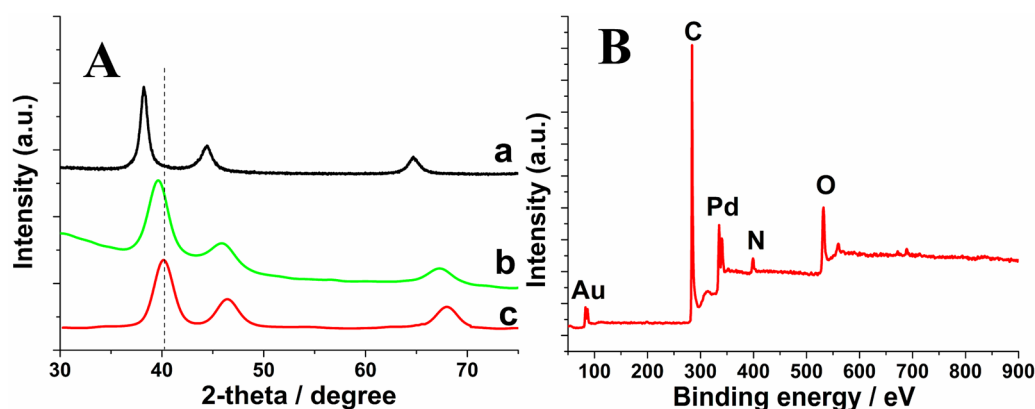

Figure 3. (A) XRD patterns of hAu (a), hAu1Pd4 (b), and hPd (c) NPs. (B) XPS spectrum of NG−hAu1Pd4 hybrid.

The mixture was stirred for 12 h at room temperature, and then centrifuged. The sediment was redispersed in 5 mL of water.

Construction of Modified Electrodes. A 3 μL as-prepared suspension was dropped onto a freshly polished GCE and let to dry in air; thus a working electrode was obtained. Working electrodes of other control groups were also fabricated by this way except that the NG−hAuPd hybrid was accordingly replaced.

■ RESULTS AND DISCUSSION

Characterization of NG−hPdAu Composite. In this paper, the hAuPd alloy NPs were prepared by exploiting the reaction between Co NPs and $PdCl_4^{2-}$ plus $AuCl_4^-$. As the standard reduction potentials of $AuCl_4^-$/Au (1.002 V vs standard hydrogen electrode (SHE)) and $PdCl_4^{2-}$/Pd (0.591 V vs SHE) are much higher than that of Co^{2+}/Co (−0.277 V vs SHE), the Co NPs were immediately oxidized to cobalt ions when the mixture of HAuCl$_4$ and Na$_2$PdCl$_4$ was added into the solution of Co NPs according to the following reaction:

$$(x + 3y/2)Co(s) + xPdCl_4^{2-}(aq) + yAuCl_4^-(aq)$$

$$\rightarrow Au_yPd_x(s) + (x + 3y/2)Co^{2+} + 4(x + y)Cl^-$$
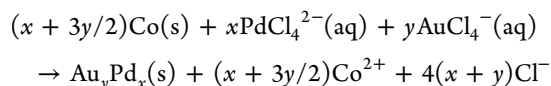
As this reaction occurred rapidly, the Pd and Au atoms nucleated simultaneously and formed very small alloy particles, eventually evolving into a thin shell around the Co NPs. The shell could have an incomplete porous structure because Co^{2+}, $PdCl_4^{2-}$, and $AuCl_4^-$ continuously diffused across the shell until the Co NPs were completely consumed. The structure and morphology of these hollow NPs were confirmed by TEM. As can be seen in Figure 2A, the hAu1Pd4 NPs displayed hollow structures and the thickness of the shell was about 2 nm. The external surface of the NPs was irregular and flower-like. The diameters of these NPs were about 25−35 nm. Meanwhile, the hollow NPs were well-dispersed on the surface of NG. The size of sAu1Pd4 NPs was similar to that of hAu1Pd4 NPs in this case (Figure S1, Supporting Information). The structure of hAu1Pd4 NPs was further investigated by the high-resolution transmission electron microscopy (HRTEM) (Figure 2B). It can be seen that the hAu1Pd4 NPs were highly crystalline with well-defined lattice fringes. The d-spacing measured at different points on a single NP was 2.26 Å, which was very close to the value of the (111) planes of face-centered cubic (fcc) Pd as the main content was Pd in the hAu1Pd4 NPs. Meanwhile, the high-angle annular dark-field scanning TEM (HAADF-STEM) image of hAu1Pd4 NPs was recorded and the distribution of each element in the NPs was obtained (Figure S2, Supporting Information). It showed that the Au and Pd atoms distributed uniformly in the whole NPs.

The composition of hAu1Pd4 NPs was determined by EDX (Figure S3, Supporting Information), and the atomic ratio of Au/Pd was about 1:4. In addition, the structure of hAu1Pd4 NPs was characterized by XRD (Figure 3A). The diffraction peaks of hAu and hPd NPs were in line with the standard peaks of Au (JCPDS 04-0784) and Pd (JCPDS 05-0681). It is worth noting that the diffraction peaks of hAu1Pd4 NPs are located
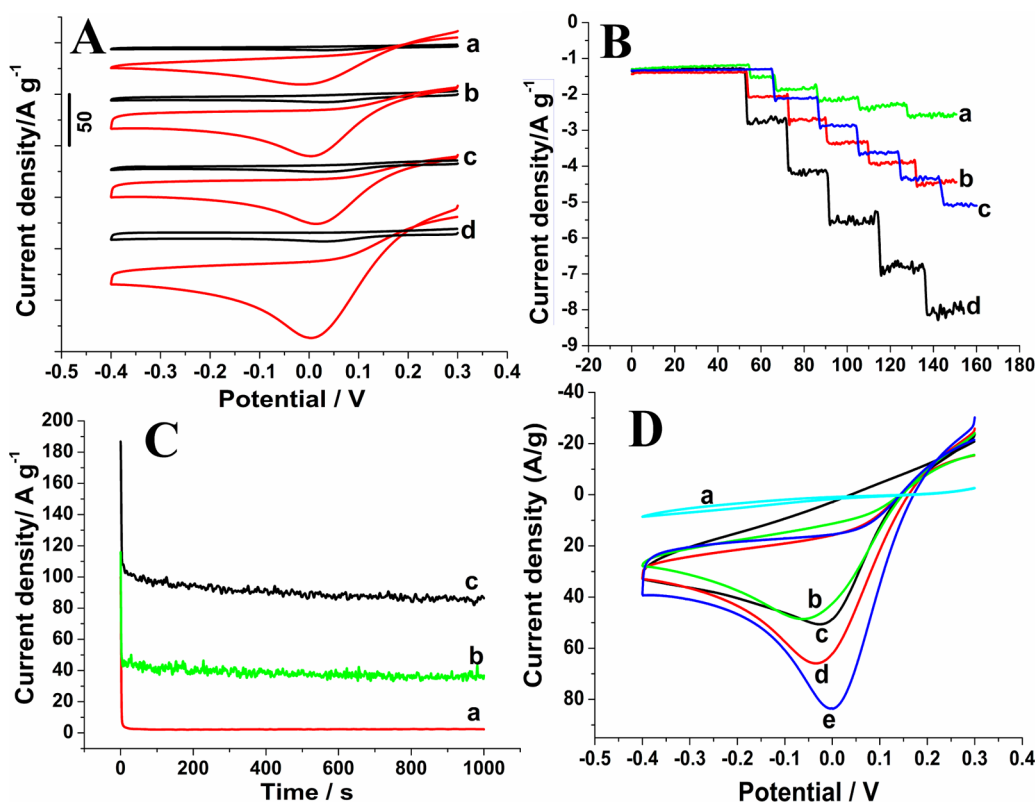
Figure 4. (A) Cyclic voltammograms (CVs) of hAu1Pd4/GCE (a), G−hAu1Pd4/GCE (b), NG−sAu1Pd4/GCE (c), and NG−hAu1Pd4/GCE (d) in 0.1 M PBS (pH 7.0) containing 0 (black) and 1 (red) mM H_2O_2. (B) Amperometric responses of hAu1Pd4/GCE (a), G−hAu1Pd4/GCE (b), NG−sAu1Pd4/GCE (c), and NG−hAu1Pd4/GCE (d) to the successive addition of 2 μM H_2O_2 at 0 V. (C) Chronoamperometric curves of NG−hAu1Pd4/GCE (a) in 0.1 M PBS (pH 7.0), hAu1Pd4/GCE (b) and NG−hAu1Pd4/GCE (c) in 0.1 M PBS (pH 7.0) containing 1 mM H_2O_2. (D) CVs of NG−hAu/GCE (a), NG−hAu1Pd2/GCE (b), NG−hPd/GCE (c), NG−hAu1Pd6/GCE (d), and NG−hAu1Pd4/GCE (e) in 0.1 M PBS (pH 7.0) containing 1 mM H_2O_2. Scan rate: 50 mV/s. All the current densities were normalized to the total mass of available Au and Pd.

between those of hAu and hPd NPs, confirming the formation of AuPd alloy rather than the mixture of monometallic NPs. On the basis of Vegard's Law (the linear lattice constant−concentration relation),[28,29] the atomic ratio of Au/Pd was estimated and it was about 1:4, which was in line with the result of EDX analysis. Furthermore, the diffraction peaks of hPd NPs were wider than that of hAu NPs, indicating the better dispersion of Pd atoms. This was in line with the previous report by Chai et al.[14] They found that, when Co NPs were oxidized by $AuCl_4^-$ and $PdCl_4^{2-}$, Au atoms predominantly occupied the interior closely spaced, while Pd atoms were inclined to occupy the surface of the NPs and were more dispersed. In this case, the content of Au was low, so the diffraction peaks of hAu1Pd4 NPs had a similar width to that of hPd NPs.

Figure S4 (Supporting Information) presents the XRD patterns of GO and NG. The feature diffraction peak of GO was at 10.4° (002), corresponding to an interlayer spacing of 0.85 nm.[30] After a solvothermal process, the pattern of the obtained NG exhibited a broad peak at 25.6°. This means that the interlayer spacing of NG sheets decreases as a certain amount of oxygen-containing groups have been removed, which is consistent with the reported XRD result of graphene sheets.[31]

The chemical composition of NG−hPdAu hybrid was also characterized by XPS measurement. The XPS survey spectra confirmed the presence of C, O, N, Pd, and Au elements (Figure 3B). However, the content of Co was too low to be

detected (Figure S5, Supporting Information). The atomic ratio of Au/Pd was about 1:4. The C/O ratio of NG was relatively higher than that of GO (Figure S6, Supporting Information), indicating the deoxygenation or reduction of GO during the reaction. These results confirmed the formation of graphene. Meanwhile, the existence of N atoms indicated the successful formation of NG. The high-resolution N 1s XPS spectrum was composed of three different types, corresponding to the pyrrolic (398.41 eV), pyridinic (399.77 eV), and graphitic (401.34) nitrogen.[23,25]
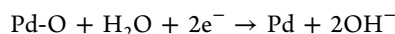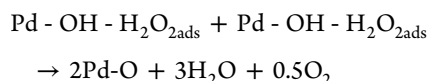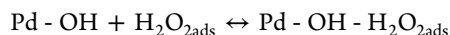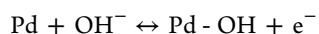
Electrocatalytic Activity toward H_2O_2 Reduction. The NG exhibited poor electrocatalysis toward the reduction of H_2O_2 (Figure S7, Supporting Information), while H_2O_2 produced an obvious reduction peak on AuPd alloy NPs modified electrodes. The electrocatalytic activity of different electrodes was compared. As shown in Figure 4A, the blank signals almost did not affect the detection of H_2O_2. When sAu1Pd4 NPs were introduced to the NG film, a large current signal appeared due to the high catalytic activity of AuPd alloy NPs.[11] When sAu1Pd4 NPs were replaced by hAu1Pd4 NPs, the current density was further enhanced. This should be ascribed to the special hollow structure of hAu1Pd4 NPs, which made the effective surface area increase. This phenomenon was in line with the previous reports.[12,13,32] For example, Hu et al.[32] synthesized hollow PtNi nanospheres for the electrooxidation of methanol and the catalyst exhibited superior electrocatalytic performance in comparison with solid PtNi nanospheres.

It should be pointed out that the cathodic peak current densities of H_2O_2 at NG−hAu1Pd4 hybrid, G−hAu1Pd4 hybrid, and hAu1Pd4 NPs modified electrodes followed such order as NG−hAu1Pd4/GCE > G−hAu1Pd4/GCE > hAu1Pd4/GCE. The reason is that graphene has a large surface area and superior conductivity and it is propitious to enhancing the availability of nanosized electrocatalysts. On the other hand, some investigations have indicated that doping N atoms in graphene can further boost its conductivity and electrochemical performance.[21−23] In this experiment, it was confirmed by the EIS (Figure S8, Supporting Information). When graphene was modified onto a GCE surface, the electron transfer resistance (R_{ct}) decreased distinctively, indicating that graphene benefited the electron transfer between the electrochemical probe $[Fe(CN)_6]^{3−/4−}$ and the electrode. After graphene was doped with N atoms, the R_{ct} further decreased, indicating that NG enhanced electron transfer efficiency. Further more, the incorporated N atoms can facilitate the interaction between graphene and metal NPs,[22] thus improving the synergistic electrocatalysis between graphene and hAu1Pd4 NPs. Owing to the better electrochemical performance of NG, the NG−hAu1Pd4/GCE exhibited higher electrocatalytic activity toward H_2O_2 reduction than G−hAu1Pd4/GCE.

The performance of different modified electrodes was further evaluated through amperometric detecting H_2O_2. Figure 4B shows the typical amperometric response curves of different nanocatalysts to the addition of H_2O_2 at 0 V vs SCE. The response time was less than 5 s, and the response current was stable. The current outputs for different electrodes followed the order of NG−hAu1Pd4/GCE > NG−sAu1Pd4/GCE > G−hAu1Pd4/GCE > hAu1Pd4/GCE.

The sensing stability of NG−hAu1Pd4/GCE was investigated by the durable chronoamperometry test (Figure 4C). As can be seen, H_2O_2 produced an obvious current signal on the NG−hAu1Pd4 hybrid, and the steady-state current density was much higher than that on hAu1Pd4 NPs, indicating that the NG−hAu1Pd4 hybrid possessed a good catalytic durability.

Figure 4D displays the CVs of 1 mM H_2O_2 at NG−hAu$_x$Pd$_y$/GCE. Compared with NG−hAu/GCE, NG−hPd/GCE exhibited an obvious reduction peak, indicating its catalytic activity toward H_2O_2 reduction. It was found that, after Au atoms were doped, the obtained AuPd alloy NPs exhibited higher catalytic activity than individual Pd NPs. This could be attributed to the synergistic effect between Au and Pd. H_2O_2 is reduced at the Pd NPs according to the following equations:[33]

$$Pd + OH^− \leftrightarrow Pd\text{-}OH + e^−$$

$$Pd\text{-}OH + H_2O_{2ads} \leftrightarrow Pd\text{-}OH\text{-}H_2O_{2ads}$$

$$Pd\text{-}OH\text{-}H_2O_{2ads} + Pd\text{-}OH\text{-}H_2O_{2ads}$$
$$\rightarrow 2Pd\text{-}O + 3H_2O + 0.5O_2$$

$$Pd\text{-}O + H_2O + 2e^− \rightarrow Pd + 2OH^−$$

When Au atoms are doped into Pd, the co-metal Au on the Pd can adsorb $OH^−$ species and enhance their concentration,[34,35] favoring the reduction of H_2O_2 absorbed on the Pd surface. However, excess incorporation of Au makes the active Pd sites decrease. In this case, the hAu1Pd4 alloy presents the highest activity.

Figure 5 shows the amperometric response of NG−hAu1Pd4/GCE to H_2O_2. A linear response range of 0.1−20 μM (linear equation: I (μA) = 0.192 + 0.36 c (μM) (R =
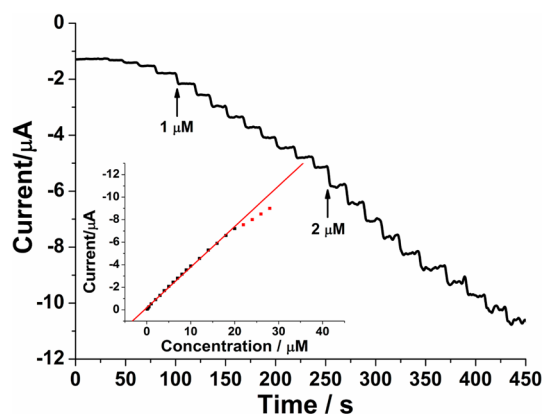
Figure 5. Amperometric response of NG−hAu1Pd4/GCE to H_2O_2 at 0 V vs SCE in 0.1 M PBS (pH = 7.0). Inset: plot of response current versus H_2O_2 concentration.

0.999)) was obtained. The detection limit was 0.02 μM (S/N = 3), and the sensitivity was estimated to be 5095.5 μA mM$^{−1}$ cm$^{−2}$. This is better than that reported for other Pd based electrodes (Table S1, Supporting Information).[1,3,6,7,33] The superior electrochemical performance of NG−hAu1Pd4/GCE should be attributed to the following reasons. First, the hollow nanostructure can offer more effective surface area and, therefore, lead to the high catalytic activity. Second, the synergistic effect between Au and Pd enhances the electrocatalytic activity of Pd toward H_2O_2. Third, chemical doping graphene with N atoms can improve the electrochemical performance of graphene and facilitate the interaction between graphene and hAuPd NPs.

In order to study the selectivity, at 0 V vs SCE, 10-fold glucose, 1-fold ascorbic acid (AA), and uric acid (UA) were added, but they showed negligible influence on the response of 5 μM H_2O_2 (Figure S9, Supporting Information). This was related to the relative low applied potential. The stability and reproducibility were also investigated. Ten successive measurements of 2 μM H_2O_2 yielded a relative standard deviation (RSD) of 3.2%. Meanwhile, after the modified electrode was scanned in PBS for 50 cycles at 50 mV/s, the peak current of H_2O_2 retained 97.7% of its initial value. After 3 weeks storage in air, the peak current retained 93.4% of its initial value for the identical concentration of H_2O_2. A RSD of 3.9% was obtained for the measurements of 2 μM H_2O_2 with seven electrodes prepared under the same conditions. This reflects the satisfactory stability and reproducibility of the catalyst.

■ CONCLUSIONS

In summary, hollow AuPd alloy NPs were prepared and loaded on nitrogen-doped graphene. The material exhibited remarkable electrocatalytic activity, satisfactory stability and reproducibility to the reduction of H_2O_2. This was correlated with the hollow structure of AuPd alloy NPs, nitrogen doping of graphene, and the synergistic effect between Au and Pd. Therefore, this work provides a promising way for preparing good catalysts for electrocatalysis and sensing applications.

■ ASSOCIATED CONTENT

ⓢ Supporting Information

TEM of sAu1Pd4 alloy NPs, XRD patterns and XPS spectra of GO and NG, EDX of Au1Pd4 alloy NPs, XPS spectra of Au, Pd, and Co in NG−hAu1Pd4 hybrid, CVs of NG/GCE in 0.1

M PBS (pH 7.0) containing 0 and 1 mM H_2O_2, Nyquist plots of GCE, G/GCE, and NG/GCE in solution containing 0.1 M KCl and 5.0 mM $Fe[(CN)_6]^{3-/4-}$ (1:1), amperometric i−t test on interference from other electroactive species at an applied potential of 0 V vs SCE, and a table about comparison of different electrodes for H_2O_2 determination. This material is available free of charge via the Internet at http://pubs.acs.org.

■ AUTHOR INFORMATION

Corresponding Author
*Tel: 86-27-68752701. Fax: 86-27-68754067. E-mail: fqzhao@whu.edu.cn (F.Z.).

Notes
The authors declare no competing financial interest.

■ REFERENCES

(1) Chen, K.-J.; Chandrasekara Pillai, K.; Rick, J.; Pan, C.-J.; Wang, S.-H.; Liu, C.-C.; Hwang, B.-J. Bimetallic PtM (M = Pd, Ir) Nanoparticle Decorated Multi-Walled Carbon Nanotube Enzyme-Free, Mediator-Less Amperometric Sensor for H_2O_2. *Biosens. Bioelectron.* **2012**, *33*, 120−127.

(2) Guascito, M. R.; Filippo, E.; Malitesta, C.; Manno, D.; Serra, A.; Turco, A. A New Amperometric Nanostructured Sensor for the Analytical Determination of Hydrogen Peroxide. *Biosens. Bioelectron.* **2008**, *24*, 1057−1063.

(3) Jiang, F.; Yue, R.; Du, Y.; Xu, J.; Yang, P. A One-Pot 'Green' Synthesis of Pd-Decorated PEDOT Nanospheres for Nonenzymatic Hydrogen Peroxide Sensing. *Biosens. Bioelectron.* **2013**, *44*, 127−131.

(4) Jia, X. E.; Hu, G. Z.; Nitze, F.; Barzegar, H. R.; Sharifi, T.; Tai, C. W.; Wagberg, T. Synthesis of Palladium/Helical Carbon Nanofiber Hybrid Nanostructures and Their Application for Hydrogen Peroxide and Glucose Detection. *ACS Appl. Mater. Interfaces* **2013**, *5*, 12017−12022.

(5) You, J. M.; Kim, D.; Kim, S. K.; Kim, M. S.; Han, H. S.; Jeon, S. Novel Determination of Hydrogen Peroxide by Electrochemically Reduced Graphene Oxide Grafted with Aminothiophenol-Pd Nanoparticles. *Sens. Actuators, B* **2013**, *178*, 450−457.

(6) Bian, X. J.; Guo, K.; Liao, L.; Xiao, J. J.; Kong, J. L.; Ji, C.; Liu, B. H. Nanocomposites of Palladium Nanoparticle-Loaded Mesoporous Carbon Nanospheres for the Electrochemical Determination of Hydrogen Peroxide. *Talanta* **2012**, *99*, 256−261.

(7) Nagaiah, T. C.; Schafer, D.; Schuhmann, W.; Dimcheva, N. Electrochemically Deposited Pd-Pt and Pd-Au Codeposits on Graphite Electrodes for Electrocatalytic H_2O_2 Reduction. *Anal. Chem.* **2013**, *85*, 7897−7903.

(8) Chen, M. S.; Kumar, D.; Yi, C. W.; Goodman, D. W. The Promotional Effect of Gold in Catalysis by Palladium-Gold. *Science* **2005**, *310*, 291−293.

(9) Zhang, L.; Wang, A.; Miller, J. T.; Liu, X.; Yang, X.; Wang, W.; Li, L.; Huang, Y.; Mou, C. Y.; Zhang, T. Efficient and Durable Au Alloyed Pd Single-Atom Catalyst for the Ullmann Reaction of Aryl Chlorides in Water. *ACS Catal.* **2014**, *4*, 1546−1553.

(10) Yang, J.; Deng, S.; Lei, J.; Ju, H.; Gunasekaran, S. Electrochemical Synthesis of Reduced Graphene Sheet−AuPd Alloy Nanoparticle Composites for Enzymatic Biosensing. *Biosens. Bioelectron.* **2011**, *29*, 159−166.

(11) Yang, F.; Cheng, K.; Wu, T.; Zhang, Y.; Yin, J.; Wang, G.; Cao, D. Au−Pd Nanoparticles Supported on Carbon Fiber Cloth as the Electrocatalyst for H_2O_2 Electroreduction in Acid Medium. *J. Power Sources* **2013**, *233*, 252−258.

(12) Wang, L.; Yamauchi, Y. Metallic Nanocages: Synthesis of Bimetallic Pt−Pd Hollow Nanoparticles with Dendritic Shells by Selective Chemical Etching. *J. Am. Chem. Soc.* **2013**, *135*, 16762−16765.

(13) Hong, J. W.; Kang, S. W.; Choi, B.-S.; Kim, D.; Lee, S. B.; Han, S. W. Controlled Synthesis of Pd−Pt Alloy Hollow Nanostructures with Enhanced Catalytic Activities for Oxygen Reduction. *ACS Nano* **2012**, *6*, 2410−2419.

(14) Chai, J.; Li, F.; Hu, Y.; Zhang, Q.; Han, D.; Niu, L. Hollow Flower-Like AuPd Alloy Nanoparticles: One Step Synthesis, Self-Assembly on Ionic Liquid-Functionalized Graphene, and Electrooxidation of Formic Acid. *J. Mater. Chem.* **2011**, *21*, 17922−17929.

(15) Li, R. S.; Hao, H.; Cai, W. B.; Huang, T.; Yu, A. S. Preparation of Carbon Supported Pd-Pb Hollow Nanospheres and Their Electrocatalytic Activities for Formic Acid Oxidation. *Electrochem. Commun.* **2010**, *12*, 901−904.

(16) Guo, S.; Dong, S.; Wang, E. Three-Dimensional Pt-on-Pd Bimetallic Nanodendrites Supported on Graphene Nanosheet: Facile Synthesis and Used as an Advanced Nanoelectrocatalyst for Methanol Oxidation. *ACS Nano* **2009**, *4*, 547−555.

(17) Gao, H.; Xiao, F.; Ching, C. B.; Duan, H. One-Step Electrochemical Synthesis of PtNi Nanoparticle-Graphene Nanocomposites for Nonenzymatic Amperometric Glucose Detection. *ACS Appl. Mater. Interfaces* **2011**, *3*, 3049−3057.

(18) Yoo, E.; Okata, T.; Akita, T.; Kohyama, M.; Nakamura, J.; Honma, I. Enhanced Electrocatalytic Activity of Pt Subnanoclusters on Graphene Nanosheet Surface. *Nano Lett.* **2009**, *9*, 2255−2259.

(19) Chen, X.; Cai, Z.; Chen, X.; Oyama, M. AuPd Bimetallic Nanoparticles Decorated on Graphene Nanosheets: Their Green Synthesis, Growth Mechanism and High Catalytic Ability in 4-Nitrophenol Reduction. *J. Mater. Chem. A* **2014**, *2*, 5668−5674.

(20) Chen, X. M.; Cai, Z. X.; Huang, Z. Y.; Oyama, M.; Jiang, Y. Q.; Chen, X. Ultrafine Palladium Nanoparticles Grown on Graphene Nanosheets for Enhanced Electrochemical Sensing of Hydrogen Peroxide. *Electrochim. Acta* **2013**, *97*, 398−403.

(21) Wang, Y.; Shao, Y.; Matson, D. W.; Li, J.; Lin, Y. Nitrogen-Doped Graphene and Its Application in Electrochemical Biosensing. *ACS Nano* **2010**, *4*, 1790−1798.

(22) Chen, S.; Duan, J.; Jaroniec, M.; Qiao, S. Z. Three-Dimensional N-Doped Graphene Hydrogel/NiCo Double Hydroxide Electrocatalysts for Highly Efficient Oxygen Evolution. *Angew. Chem., Int. Ed.* **2013**, *52*, 13567−13570.

(23) Mahmood, N.; Zhang, C.; Hou, Y. Nickel Sulfide/Nitrogen-Doped Graphene Composites: Phase-Controlled Synthesis and High Performance Anode Materials for Lithium Ion Batteries. *Small* **2013**, *9*, 1321−1328.

(24) Prabu, M.; Ramakrishnan, P.; Shanmugam, S. $CoMn_2O_4$ Nanoparticles Anchored on Nitrogen-Doped Graphene Nanosheets as Bifunctional Electrocatalyst for Rechargeable Zinc-Air Battery. *Electrochem. Commun.* **2014**, *41*, 59−63.

(25) Mahmood, N.; Zhang, C.; Liu, F.; Zhu, J.; Hou, Y. Hybrid of Co_3Sn_2@Co Nanoparticles and Nitrogen-Doped Graphene as a Lithium Ion Battery Anode. *ACS Nano* **2013**, *7*, 10307−10318.

(26) Bai, J. C.; Zhu, Q. Q.; Lv, Z. X.; Dong, H. Z.; Yu, J. H.; Dong, L. F. Nitrogen-Doped Graphene as Catalysts and Catalyst Supports for Oxygen Reduction in Both Acidic and Alkaline Solutions. *Int. J. Hydrogen Energy* **2013**, *38*, 1413−1418.

(27) Xiong, B.; Zhou, Y. K.; O'Hayre, R.; Shao, Z. P. Facile Single-Step Ammonia Heat-Treatment and Quenching Process for the Synthesis of Improved Pt/N-Graphene Catalysts. *Appl. Surf. Sci.* **2013**, *266*, 433−439.

(28) Klug, H. P.; Alexander, L. E. *X-Ray Diffraction Procedures for Polycrystalline and Amorphous Materials*; Wiley: New York, 1974.

(29) Jenkins, R.; Snyder, R. L. *Introduction to X-Ray Powder Diffractometry*; Wiley: New York, 1996.

(30) Jeong, H.-K.; Lee, Y. P.; Lahaye, R. J. W. E.; Park, M.-H.; An, K. H.; Kim, I. J.; Yang, C.-W.; Park, C. Y.; Ruoff, R. S.; Lee, Y. H. Evidence of Graphitic Ab Stacking Order of Graphite Oxides. *J. Am. Chem. Soc.* **2008**, *130*, 1362−1366.

(31) Parvez, K.; Yang, S.; Hernandez, Y.; Winter, A.; Turchanin, A.; Feng, X.; Müllen, K. Nitrogen-Doped Graphene and Its Iron-Based

Composite as Efficient Electrocatalysts for Oxygen Reduction Reaction. *ACS Nano* **2012**, *6*, 9541−9550.

(32) Hu, Y.; Shao, Q.; Wu, P.; Zhang, H.; Cai, C. Synthesis of Hollow Mesoporous Pt−Ni Nanosphere for Highly Active Electrocatalysis toward the Methanol Oxidation Reaction. *Electrochem. Commun.* **2012**, *18*, 96−99.

(33) Jamal, M.; Hasan, M.; Mathewson, A.; Razeeb, K. M. Non-Enzymatic and Highly Sensitive H_2O_2 Sensor Based on Pd Nanoparticle Modified Gold Nanowire Array Electrode. *J. Electrochem. Soc.* **2012**, *159*, B825−B829.

(34) Geraldes, A. N.; da Silva, D. F.; Pino, E. S.; da Silva, J. C. M.; de Souza, R. F. B.; Hammer, P.; Spinacé, E. V.; Neto, A. O.; Linardi, M.; dos Santos, M. C. Ethanol Electro-Oxidation in an Alkaline Medium Using Pd/C, Au/C and PdAu/C Electrocatalysts Prepared by Electron Beam Irradiation. *Electrochim. Acta* **2013**, *111*, 455−465.

(35) Lv, Z.-Y.; Fei, Y.; Chen, W.-Y.; Tan, Y.-F.; Sun, C.-Q.; Chen, J.-R.; Wang, A.-J.; Feng, J.-J. Hierarchical Wheat-like Au−Pd Heterostructures with Enhanced Catalytic Activity toward Methanol Electrooxidation. *J. Alloys Compd.* **2013**, *581*, 717−723.